ELSEVIER

Journal of Molecular Catalysis A: Chemical 152 (2000) 213–223

JOURNAL OF MOLECULAR CATALYSIS A: CHEMICAL

www.elsevier.com/locate/molcata

Nitrobenzene hydrogenation on Ni–P, Ni–B and Ni–P–B ultrafine materials

Shao-Pai Lee, Yu-Wen Chen *

Department of Chemical Engineering National Central University, Chung-Li 32504, Taiwan

Received 13 February 1999; received in revised form 6 August 1999; accepted 6 August 1999

Abstract

A series of ultafine Ni–P, Ni–B and Ni–P–B amorphous alloy catalysts with various atomic ratios was prepared by a chemical reduction method. The catalysts were characterized with respect to nitrogen sorption, X-ray diffraction (XRD), transmission electron microscopy (TEM), inductively coupled plasma-atomic emission spectroscopy (ICP-AES), X-ray photoelectron spectroscopy (XPS) and hydrogenation activity. Conventional Raney nickel was included for comparison. The Ni/P/B molar ratios in the starting materials significantly affects the concentration of boron and phosphorus bonded to the nickel metal, subsequently affecting the surface area, amorphous structure and hydrogenation activity of the catalysts. The prepared catalyst, although easily degraded by gaseous oxygen, did not ignite in the atmosphere due to the passivation by phosphorus and boron. The hydrogenation of nitrobenzene to aniline catalyzed actively by the Ni–P–B, Ni–B and Ni–P amorphous alloy catalysts, following the zeroth order with respect to nitrobenzene and first order with respect to hydrogen kinetics. The specific activities per surface area catalyst are in the following order: $Ni_{85.0}P_{15.0} > Ni_{74.5}P_{12.1}B_{13.4} > Ni_{72.5}P_{2.0}B_{25.5} > Ni_{71.4}B_{28.9} > Ni_{78.5}P_{6.0}B_{15.5}$ > Raney nickel. The modified nickel catalysts by the different electron transference, boron donates electrons to nickel and phosphorus draws electrons from nickel, depending on the different function groups of the reaction compounds, dramatically reveals a markedly different property of catalysis. By regulating the suitable P/B ratios, the ultrafine Ni–P–B amorphous alloy catalysts can be a very effective catalyst for the various liquid phase hydrogenation reaction than Raney nickel.

Keywords: Ni–P–B ultrafine amorphous alloy catalyst; Nitrobenzene hydrogenation; Nanomaterial

1. Introduction

The ultrafine amorphous alloy powders combine the features of amorphous and ultrafine powders, have more surface atoms and a higher concentration of highly coordinated unsaturated sites. Their unique isotropic structural and chemical properties have attracted extensive interest in recent years [1–11]. Previous investigators reported such a combination to create properties, particularly for catalytic and magnetic recording applications [12–14]. However, the catalytic properties of these materials have seldom been investigated. Okamoto et al. [13,28,29] characterized the surface of Ni–B and Ni–P ultrafine catalysts prepared by a chemical reduction method with X-ray photoelectron spectroscopy (XPS), indicating that a variation in 3d electron density on the nickel metal induced by

* Corresponding author. Fax: +886-3-4252296; e-mail: ywchen@cc.ncu.edu.tw

1381-1169/00/$ - see front matter
PII: S1381-1169(99)00298-8

boron or phosphorus would modify the activity and selectivity of the nickel catalyst for hydrogenation. Shen et al. [15] successfully prepared Ni–P–B ultrafine amorphous particles by chemical reduction methods. As generally known, boron or phosphorus will affect the surface properties of these catalysts and, hence, their catalytic properties. The Ni–P–B ultrafine amorphous alloy powders, which consists the effects of two metalloid elements (B, P) and the feature of ultrafine amorphous structure, has seldom been mentioned the property of reaction and surface state. The determination of surface stoichiometry and chemical states of the surface plays a most important role in understanding the activity of the catalysts. In our previous study, it was found that the different electron transfer between nickel metal and the metalloid elements in Ni–P and Ni–B powders, results in the extremely different activity and selectivity for the hydrogenation of furfural. By regulating suitable P/B ratio, the ultrafine Ni–P–B catalyst appeared in the different surface electrons states from Ni–P and Ni–B powders, and dramatically revealed a markedly higher hydrogenation activity of furfural than Ni–P and Ni–B. In this study, nitrobenzene hydrogenation was chosen to further investigate the hydrogenation capabilities and the surface properties of these ultrafine Ni–P_x–B_y catalysts, including Ni–P, Ni–B and Ni–P–B.

Hydrogenation of nitrobenzene has been known to be an important industrial process [16–20]. It is usually catalyzed by two classes of solids: noble metals, such as platinum, palladium, ruthenium, rhodium; and Raney metals, such as Raney nickel. In this study, a series of ultrafine Ni–P, Ni–B and Ni–P–B amorphous alloy catalysts with various atomic ratios was prepared. The catalysts were characterized with respect to nitrogen sorption, X-ray diffraction (XRD), transmission electron microscopy (TEM), inductively coupled plasma-atomic emission spectroscopy (ICP-AES), XPS and hydrogenation activity. Commercial Raney nickel was included for comparison.

2. Experimental

2.1. Chemicals

Nitrobenzene, with a purity of $>99\%$, was obtained from Merck (St. Louis, MO). High purity hydrogen gas ($>99.99\%$) from Sanfu Gas (Taiwan) was used without further purification. Nickel acetate tetrahydrate ($>98\%$) was supplied by Showa Chemicals (Tokyo, Japan). Sodium hypophosphite ($>99\%$) was obtained from Fisher (NJ, USA) Sodium borohydride ($>98\%$) was purchased from Lancaster (Morecambe, UK).

2.2. Catalyst preparation

A series of Ni–P–B catalysts with various Ni/P/B molar ratios and Ni–B, Ni–P catalysts was prepared by chemical reaction methods. The Ni–P_x–B_y amorphous alloy powders were prepared by mixing an aqueous solution of nickel acetate (1000 ml, 0.1 M) and sodium hypophosphite (1 M) at 30°C under ultrasonic agitation. The solution of sodium borohydride (0.1 M) was then added dropwisely into the mixture. The black precipitates which subsequently formed were washed thoroughly with a large amount of distilled water, followed by an ethanol rinse, and soaked in 99% ethanol. The Ni–B powder was prepared by a similar method with the Ni–P–B powders in the absence of sodium hypophosphite. The Ni–P powder was prepared by heating up an aqueous solution that consists of 25.4 g nickel acetate and 31.8 g sodium hypophosphite at 70°C with a vigorous stirring. The pH value of solution was adjusted to 11 using 30 wt.% NaOH aqueous solution. The NiP black precipitate was washed with 8 M aqueous ammonia, then washed with distilled water and followed by ethanol, also soaked in ethanol. The commercial Raney nickel was obtained from Strem Chemicals. It has 85 wt.% Ni and 15 wt.% Al.

2.3. Catalyst characterization

Elemental analysis using ICP-AES (Jobin-Yvon, France, JY-24) was performed on the Ni–P–B materials. In general, the weighted samples were dissolved in nitric acid and diluted with distilled water to the concentration within the calibration range of each element. The standard solutions purchased from Merck were diluted and used to establish the calibration curves. Wavelengths in nm used for elemental analysis were 231.604, 214.914 and 249.773 for Ni, P and B, respectively.

XRD measurements were taken using a Siemens D5000 powder diffractometer with Cu-Kα radiation (40 kV, 30 mA). The sample was scanned over the range $2\theta = 5$–80°C to identify the amorphous structure. The morphologies and particle sizes of the samples were determined by TEM performed on a Jeol JEM-1200 EX II electron microscope operating 160 kV. After an etching of the surface by Ar^+ ions for 30 s, the XPS spectra were recorded with a Perkin Elmer PHI-1600 photoelectron spectrometer using Mg Kα radiation (15 kV and 25 mA). The base pressure in the analyzing chamber was maintained on the order of 10^{-9} Torr. The spectrometer was operated at 23.5 eV pass energy. The catalyst sample was mounted quickly onto a grid attached to a sample holder, keeping the powder soaked in 99% ethanol to minimize the oxidation of the powder by air. After evacuating the ethanol, the sample was transferred to the analyzing chamber. The BET surface area was measured by nitrogen volumetric adsorption (Micromeritics ASAP 2000) at -196°C. The temperature of the liquid nitrogen bath was checked by a thermistor probe.

2.4. Reaction setup

All the experiments were carried out in a cylindrical stirred-tank reactor (Parr Instrument Model 4842), with 150 mm height, 63.5 mm internal diameter, and 300 ml capacity. A four-bladed pitched impeller was placed for effective agitation, and the agitator was connected to an electric motor with variable speed up to 1700 rpm. A pressure transmitter and an automatic temperature controller were also provided. The gases were supplied from cylinders and introduced to the base of the reactor, the entrance tube also served as a sampling tube for the liquid phase.

2.5. Reaction procedure

The catalytic activities of the samples were tested by the hydrogenation of nitrobenzene to aniline in cyclohexane solution. The reactor was charged with 0.3 g catalyst, and 5 ml nitrobenzene in 170 ml cyclohexane solution. Air was flushed out of the reactor with nitrogen at room temperature, hydrogen was then fed into the reactor. Next, the inlet valve was closed and heating commenced with stirring to avoid settling of the catalyst. When the designated temperature 125°C was reached, hydrogen was fed to the predetermined pressure 100 psig (time zero) which was maintained throughout the reaction, the stirrer speed was 1700 rpm. During the run, samples (0.5 ml each) were withdrawn periodically and analyzed by a gas chromatograph. A gas chromatograph equipped with flame ionization detector and a 2 m $\times$ 1/8 in. (1 in. = 2.54 cm) stainless steel column packed with 3% OV-17 on Chromosob W-HP (80–100 mesh) was used for sample analysis. Nitrogen was used as a carrier gas.

A polynomial equation was fitted to the conversion data for each set of reaction conditions. Differential of the best fit equation (the zero-order reaction is linear equation) directly gave the hydrogenation rate r ($\mathrm{d}x/\mathrm{d}t$). The value of the initial rate was obtained by calculating the rate at the zero time.

3. Results and discussion

3.1. Catalyst characterization

Table 1 lists the compositions, surface areas and particle sizes of the catalysts samples. The

compositions of the samples were determined by XPS (surface atomic composition) and ICP-AES (bulk atomic composition). The data indicate that the surface stoichiometry were identical to the bulk for Ni–B powder and Ni–P powder, but the Ni–P–B powders are not. The difference between surface stoichiometry and bulk for Ni–B–P powders can be attributed to the mechanism [15] of the two competing reactions between metalloids ($H_2PO_2^-$, BH_4^-) and nickel ion (Ni^+). In synthesis, the composition was determined by the relative rates of reactions (i) and (ii). Therefore, it is possible that the rate of two reactions did not maintain constant throughout the reaction process; however, the difference were not great.

$$2H_2PO_2^- + 2H_2O + Ni^{2+} \rightarrow Ni\downarrow + H_2\uparrow + 4H^+ + 2HPO_3^{2-} \quad \text{(i)}$$

$$4BH_4^- + 2Ni^{2+} + 9H_2O \rightarrow Ni_xB\downarrow + 3H_3BO_3 + 12.5H_2\uparrow \quad \text{(ii)}$$

The surface compositions of the samples determined by XPS were sample (A) $Ni_{71.4}B_{28.9}$ (mole %) for Ni–B powder, sample (B) $Ni_{85.0}P_{15.0}$ (mole %) for Ni–P powder and sample (C) $Ni_{72.5}P_{2.0}B_{25.5}$ (mole %), sample (D) $Ni_{78.5}P_{6.0}B_{15.5}$ (mole %), sample (E) $Ni_{74.5}P_{12.1}B_{13.4}$ (mole %) for Ni–P–B powders. The composition significantly influenced the surface area of the sample. The sample (A) $Ni_{71.4}B_{28.9}$ for Ni–B powder had the largest surface area (38.8 m^2/g). The sample (B) $Ni_{85.0}P_{15.0}$ for Ni–P powder had the smallest surface area (3.3 m^2/g). The sample (C) $Ni_{72.5}P_{2.0}B_{25.5}$, sample (D) $Ni_{78.5}P_{6.0}B_{15.5}$ and sample (E) $Ni_{74.5}P_{12.1}B_{13.4}$ for Ni–P–B powders had a middle surface area (22.7 m^2/g, 32.1 m^2/g and 15.1 m^2/g, respectively) between Ni–B powder and Ni–P powder. The surface area of sample (F) Raney nickel $Ni_{72.3}Al_{27.7}$ was 59.4 m^2/g.

Owing to the different starting concentrations of boron and phosphorous, the distinct differences of the morphology and particle size among these samples were observed in TEM micrograph. The sample (B) Ni–P powder has a spherical morphology, and the diameter is about 50–150 nm. The sample (A) $Ni_{71.4}B_{28.9}$ for Ni–B powder and samples (C) $Ni_{72.5}P_{2.0}B_{25.5}$, (D) $Ni_{78.5}P_{6.0}B_{15.5}$, (E) $Ni_{74.5}P_{12.1}B_{13.4}$ for Ni–P–B powders, have a markedly smaller size than Ni–P, with a similar diameter ranging from 10 to 30 nm (Table 1). Furthermore, by assuming that the sample particles are spherical and nonporous, their average sizes can be estimated by the formula $\bar{d}(\text{nm}) = (6/S_{\text{BET}}\rho)10^3$ where S_{BET} denotes the surface area and ρ represents the density of a particle using the value of 8.9 g/cm^3 (the density of nickel). Results of parti-

Table 1
The characteristics of the catalysts on the composition, surface area and particle size

Catalyst samples (Ni:P:B mole ratio initial prep.)[a]	XPS[b] composition (atomic ratio)	ICP[c] Bulk composition (atomic ratio)	BET surface area (m^2/g)	Particle size (nm)	
				TEM measured	Estimated average size
(A) Ni–B (1:0:3)	$Ni_{71.4}B_{28.9}$	$Ni_{69.3}B_{30.7}$	38.8	10–30	17
(B) Ni–P (1:3:0)	$Ni_{85.0}P_{15.0}$	$Ni_{83.5}P_{16.5}$	3.3	50–150	204
(C) Ni–P–B (1:0.3:3)	$Ni_{72.5}P_{2.0}B_{25.5}$	$Ni_{69.4}P_{1.0}B_{29.6}$	22.7	10–30	30
(D) Ni–P–B (1:3:3)	$Ni_{78.5}P_{6.0}B_{15.5}$	$Ni_{80.7}P_{8.0}B_{11.3}$	32.1	10–30	21
(E) Ni–P–B (1:3:1)	$Ni_{74.5}P_{12.1}B_{13.4}$	$Ni_{82.0}P_{9.1}B_{8.9}$	15.1	10–30	45

[a] Ni:P:B mole ratio in the mother solution.
[b] Ni:P:B atomic ratio in the surface of the ultrafine material.
[c] Ni:P:B atomic ratio in the bulk of the ultrafine material.

cle size from TEM micrograph and estimated value (listed in Table 1) resemble each other.

The XRD patterns of the prepared samples as shown in Fig. 1 gave only a broad peak around $2\theta = 45°$. This was assigned to the amorphous state of nickel-metalloid alloy [21]. Notably, the patterns contained no distinct peak corresponding to a crystalline phase. Comparing the XRD patterns of Ni–P–B, Ni–B and Ni–P sample reveals an obvious difference, indicating that Ni–B powder has a wider disorder range than Ni–P–B powder, and Ni–P–B powder than Ni–P powder. Moreover, the extent of the wider disorder range increased with a decrease of phosphorus contents in the amorphous samples.

The XPS spectra of Ni–B, Ni–P and Ni–P–B powders are shown in Fig. 2. The $Ni_{2p_{3/2}}$ binding energy for all the Ni–B, Ni–P and Ni–P–B powders at 852.3–852.5 eV, comparing with the spectrum of pure nickel metal 852.2 eV, is ascribed to metallic Ni [13–15,28,29]. In the B_{1s} level, there exist two kinds of boron species on the surface of Ni–B and all the Ni–P–B powders. The peaks at the lower and higher binding energy are assigned to boron interacting with nickel (187.9–188.1 eV, for the Ni–B and all the Ni–P–B powders) and oxidized boron (192.7–193.0 eV, for the Ni–B and all the Ni–P–B powders), respectively. The lower binding energy at 187.9–188.1 eV shifted positively from elementary boron (186.5–187.0 eV), it is concluded that the boron species interacting with nickel are positively charged and the boron donates electrons [13,14,28,29]. In the P_{2p} level, two kinds of phosphorous species appeared on the surface of Ni–P and all the Ni–P–B powders. The peaks at the lower and higher binding energy are assigned to phosphorous interacting with nickel (129.5–129.7 eV, for the Ni–P and all the Ni–P–B powders) and oxidized phosphorus (133.3–133.6 eV, for the Ni–P and all the Ni–P–B powders), respectively. The lower binding energy peak at 129.5–129.7 eV shifted negatively by 0.7–0.9 eV from red phosphorous (130.4 eV), it is concluded that the phosphorous species interacting with nickel are positively charged and the phosphorus accepts electrons [13,14,28,29], similar negative shifts have been reported [30] for MnP (−0.8 eV), CrP (−1.3 eV) and Cu_3P (−0.4 eV). Furthermore, the XPS data of Ni–P–B, Ni–P and Ni–B powders reveal that the significantly different electron

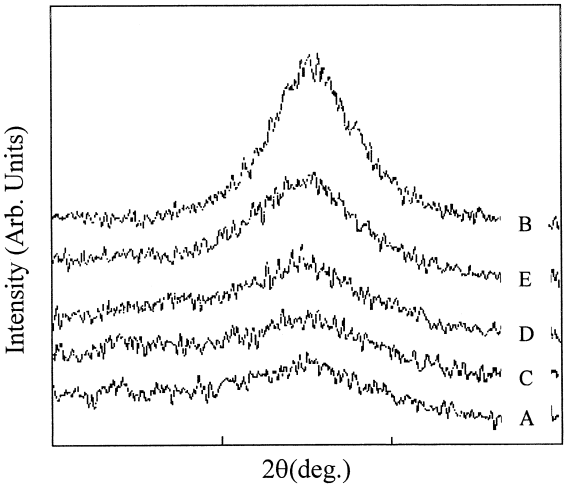

Fig. 1. XRD patterns of Ni–P–B, Ni–P and Ni–B samples. (B) $Ni_{85.0}P_{15.0}$. (E) $Ni_{74.5}P_{12.1}B_{13.4}$. (D) $Ni_{78.5}P_{6.0}B_{15.5}$. (C) $Ni_{72.5}P_{2.0}B_{25.5}$. (A) $Ni_{71.4}B_{28.9}$.

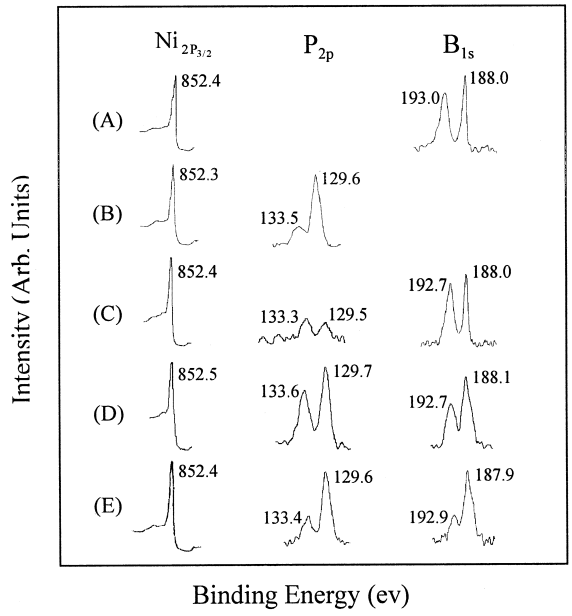

Fig. 2. XPS spectra of Ni–B, Ni–P and Ni–P–B Samples (A) $Ni_{71.4}B_{28.9}$. (B) $Ni_{85.0}P_{15.0}$. (C) $Ni_{72.5}P_{2.0}B_{25.5}$. (D) $Ni_{78.5}P_{6.0}B_{15.5}$. (E) $Ni_{74.5}P_{12.1}B_{13.4}$.

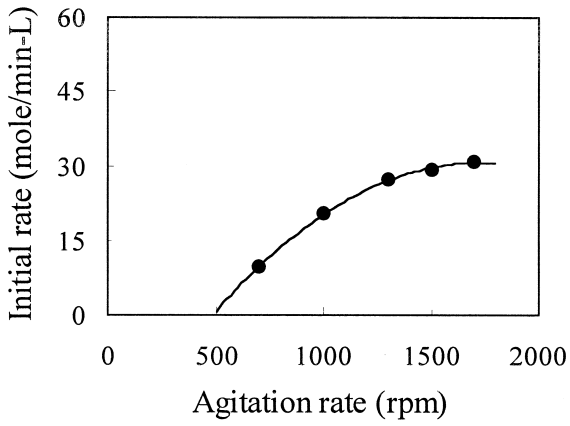

Fig. 3. Effect of agitation rate on the initial rate of hydrogenation of nitrobenzene. (Reaction conditions: catalyst, $Ni_{72.5}P_{2.0}B_{25.5}$, 0.3 g; temperature, 125°C; pressure, 100 psig.)

transference between nickel metal and the metalloids were existing among the ultrafine Ni–B, Ni–P and Ni–P–B powders. Boron combined with nickel metal in the Ni–B powder was found to donate electrons to the nickel metal, whereas phosphorus bonded to nickel metal accepted electrons from the nickel metal. The electron transference between nickel and metalloids in the Ni–P–B powder is complex; the different electron transference between nickel and metalloid elements, boron donates electrons and phosphorus draws electrons, are existing at the same time.

3.2. Mass-transfer considerations

The plot of initial reaction rate versus agitation rate is shown in Fig. 3. The need for the higher agitation rate (1700 rpm, the maximum agitation rate for the reactor) may be due to the different properties of hydrophillic catalysts and oil solution, the hydrophillic catalysts were not easily scattered in the oil solution (such as cyclohexane). In this study, 1700 rpm was used in all the reaction studies. Catalytic reaction in a slurry reactor involves processes such as gas-to-liquid mass transfer, liquid-to-particle mass transfer, intraparticle diffusion, adsorption, surface reaction, and desorption of products [22]. To evaluate the extent of mass-transfer limitation related to diffusion from the liquid to the solid phase and within the catalyst particles, the methods introduced by Carberry [23], Wheeler [24], and Weisz and Prater [25] have been adopted. The Carberry number, $Ca = r_{obs}/(k_{1s}(6w/d_p\,\rho_p)C)$, represents the extent of external mass-transfer limitation and ranges from zero to unity. A Carberry number smaller than 0.05 indicates that diffusion retardation by external mass transfer may be neglected. The Wheeler–Weisz group, $\eta\varphi^2 = (d_p^2 r_{obs})/4D_{eff}V_pC)$, represents the extent of pore diffusion limitation and range from zero to infinity; where r_{obs} = observed rate (mol/s), k_{1s} = liquid/solid mass-transfer coefficient (m/s), w = catalyst weight (g), d_p = mean particle size (m), ρ_p = catalyst apparent density (g/cm^3), C = solubility (mol/cm^3), D_{eff} = diffusion coefficient (m^2/s), and V_p = catalyst volume (cm^3). A value of the group smaller than 0.1 means that pore diffusion limitation is negligible. These ultrafine catalysts have very small particle size ($d_p \leq 100$ nm). The Carberry num-

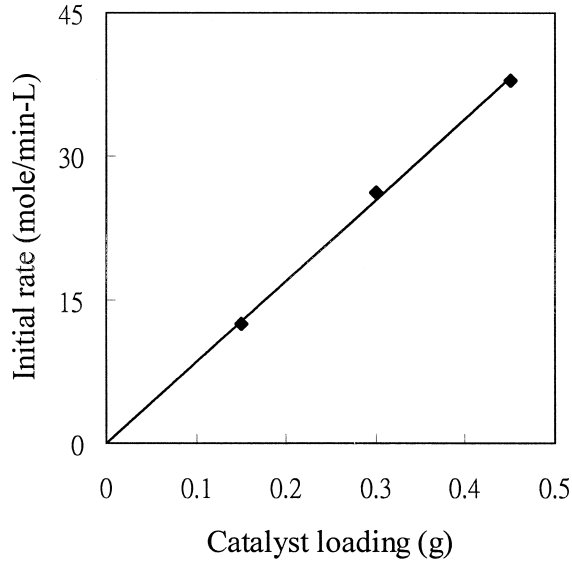

Fig. 4. Effect of catalyst loading on the initial rate of hydrogenation of nitrobenzene. (Reaction conditions: catalyst, $Ni_{72.5}P_{2.0}B_{25.5}$; temperature, 125°C; pressure, 100 psig; stirrer speed, 1700 rpm.)

ber *Ca* and the Wheeler–Weisz group $\eta\varphi^2$ are directly proportional to d_p and d_p^2, respectively. The values of *Ca* and $\eta\varphi^2$ are very small ($Ca < 0.05$, $\eta\varphi^2 < 0.1$). In addition, These ultrafine catalysts are nonporous as evidenced by the low BET surface area. Therefore, the mass-transfer limitations related to diffusion from the liquid to the solid phase and within the catalyst particles are neglected. The gas–liquid mass-transfer limitation can be eliminated by the proper stirring speed [26]. This can be verified by a series of experiments carried out using different amounts of catalysts [27]. Fig. 4 shows the effect of catalyst loading on the initial rate of hydrogenation of nitrobenzene at 125°C. The rate is linearly dependent on the catalyst loading with zero intercept. This observation suggests that gas–liquid mass-transfer resistance is not important under this condition. Therefore, one can conclude that the reactions were carried out under a kinetic-controlled regime.

3.3. Reaction kinetics

Typical plots of nitrobenzene conversion versus time are shown in Fig. 5. In this study,

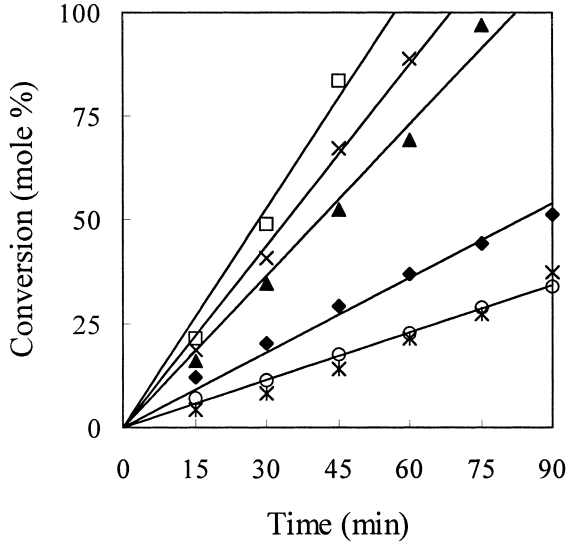

Fig. 5. Conversion-time curves for the disappearance of nitrobenzene, catalyzed by the wet catalyst samples. □(C) $Ni_{72.5}P_{2.0}B_{25.5}$. ×(A) $Ni_{71.4}B_{28.9}$. ▲(E) $Ni_{74.5}P_{12.1}B_{13.4}$. ◆(D) $Ni_{78.5}P_{6.0}B_{15.5}$. ○(F) Raney nickel. ∗(B) $Ni_{85.0}P_{15.0}$.

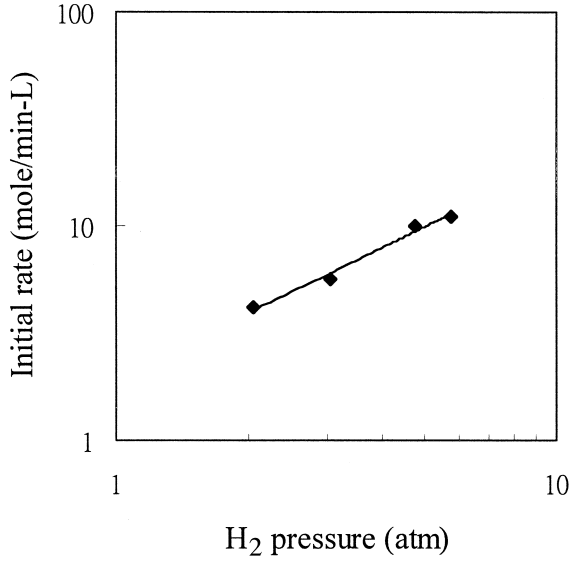

Fig. 6. The typical plot of the hydrogenation reaction rate of nitrobenzene versus hydrogen partial pressure on the Ni–P_x–B_y catalysts. (Reaction conditions: catalyst, $Ni_{72.5}P_{2.0}B_{25.5}$; temperature, 125°C; stirrer speed, 1700 rpm.)

aniline is the primary product. The selectivity to aniline on all the catalysts was greater than 99%. In contrast, Burge et al. [19] reported a significant amount of intermediates such as predominantly azobenzene and azoxybenzene was produced on Raney nickel. The discrepancy is due to the different solvent.

Fig. 5 shows that the reaction is zeroth order with respect to nitrobenzene, while Fig. 6 shows the reaction is first order with respect to the partial pressure of hydrogen. Most of the results of liquid-phase hydrogenation of nitrobenzene in the literature [16–20] show that the reaction is zeroth order with respect to nitrobenzene and first order with respect to hydrogen. Our results are in accord with this. The reaction kinetics can be described as $-r_{\text{nitrobenzene}} = kP_{H_2}$, where $-r_{\text{nitrobenzene}}$ is the disappearance rate of nitrobenzene, k is the rate constant, and P_{H_2} is partial pressure of hydrogen. In a previous paper, one of the authors [31] has concluded that this reaction can be described by the Langmuir–Hinshelwood model. The rate determining step is the surface reaction between nitrobenzene and hydrogen, and two hydrogen

atoms are involved in the surface reaction. Aramendia et al. [17] and Metcalfe and Rowden [20] reached the same conclusion. Therefore, the reaction kinetics can be described as $-r_{\text{nitrobenzene}} = k'(\theta_H)^2$, where k' is the rate constant and θ_H is the surface coverage by hydrogen atoms.

3.4. Catalytic hydrogenation activity

Table 2 lists the reaction activities of the hydrogenation of nitrobenzene to aniline catalyzed by ultrafine Ni–P–B, Ni–B and Ni–P amorphous alloy catalysts. The order of catalytic activity per weight of the catalyst was sample (C) $Ni_{72.5}P_{2.0}B_{25.5}$ > sample (A) $Ni_{71.4}B_{28.9}$ > sample (E) $Ni_{74.5}P_{12.1}B_{13.4}$ > sample (D) $Ni_{78.5}P_{6.0}B_{15.5}$ > sample (F) $Ni_{72.3}Al_{27.7}$ (Raney nickel) > sample (B) $Ni_{85.0}P_{15.0}$. The specific catalytic activity per surface area is in the order: sample (B) $Ni_{85.0}P_{15.0}$ > sample (E) $Ni_{74.5}P_{12.1}B_{13.4}$ > sample (C) $Ni_{72.5}P_{2.0}B_{25.5}$ > sample (A) $Ni_{71.4}B_{28.9}$ > sample (D) $Ni_{78.5}P_{6.0}B_{15.5}$ > sample (F) $Ni_{72.3}Al_{27.7}$ (Raney nickel). The results demonstrated that Ni–P ultrafine materials have a higher specific catalytic activity per surface area in the liquid phase hydrogenation reaction of nitrobenzene than Ni–P–B, and Ni–P–B than Ni–B.

The differences among the catalytic activities can be attributed to the difference of the electron density on the nickel metal among Ni–P–B, Ni–P and Ni–B catalysts [13–15,28,29]. Comparing the XPS data of Ni–P–B, Ni–P and Ni–B catalysts reveals that boron combined with nickel metal in Ni–B powder would donate electrons to the nickel metal, resulting in electron rich nickel metal. Whereas phosphorus bonded to nickel metal in Ni–P powder would accept electrons from the nickel metal, causing electron deficient metal. The significantly different transference between the nickel metal and the metalloids, phosphorus draws electrons and boron donates electrons, results in the markedly different hydrogenation activity of nitrobenzene (specific activity per surface area: $Ni_{85.0}P_{15.0}$ > $Ni_{71.4}B_{28.9}$). In the Ni–P–B powder, the modification of electron density on the nickel metal was not the same with Ni–P and Ni–B powders. The different electron transference between nickel (Ni) and metalloids (B, P), boron donates electrons to nickel and phosphorus draws electrons from nickel, are existing at the same time. The fact that the electron transference between nickel and metalloids in the Ni–P–B catalyst is complex, reflecting why the mechanism is still not completely understood. However, the modification of boron and phosphorous on the hydrogenation activities of Ni–P–B catalysts can be ascribed to the modification of electron density on the nickel metal. The Ni–P–B powders reveal a markedly different hydrogenation activity with the different P/B ratios, but it had no regularization with the contents of boron and phosphorus.

Considering the results of the other studies. Okamoto et al. [13] indicated the specific activities for the hydrogenation of cyclohexene and cyclo-octene, increasing with increasing surface boron content in Ni–B catalysts, whereas they decreased with increasing surface phosphorous content in Ni–P catalysts. Deng et al. [14] indicated that the specific activities per surface area for the hydrogenation of 1,3-cyclopentadiene to cyclopentene on Ni–B catalyst similar to that on Ni–P catalyst, and further concluded that the different electron transference between nickel and metalloid elements (P, B) does not result in

Table 2
The initial activities of Ni–P–B, Ni–P and Ni–B catalysts

Catalyst samples	Catalytic activities	
	$\text{mol}\cdot H_2\cdot(\text{m}^2\ \text{Cat.})^{-1}\cdot S^{-1}\times 10^3$	$\text{mol}\cdot H_2\cdot(\text{gNi})^{-1}\cdot S^{-1}\times 10^2$
(A) $Ni_{71.4}B_{28.9}$	6.6	27.3
(B) $Ni_{85.0}P_{15.0}$	18.3	6.7
(C) $Ni_{72.5}P_{2.0}B_{25.5}$	10.9	30.9
(D) $Ni_{78.5}P_{6.0}B_{15.5}$	3.3	10.5
(E) $Ni_{74.5}P_{12.1}B_{13.4}$	12.2	19.8
(F) $Ni_{72.3}Al_{27.7}$ (Raney nickel)	1.1	7.4

distinct change of the active site. In this study, the experiment results show that the specific activities per surface area for the hydrogenation of nitrobenzene on these ultrafine Ni–P_x–B_y powders was $Ni_{85.0}P_{15.0} > Ni_{71.4}B_{28.9}$, and the ultrafine Ni–P–B powders reveal a markedly different hydrogenation activity with the different P/B ratios. The discrepancy among these studies may be due to the different interactions between the different function groups of reaction compounds and the modified nickel by metalloids (P, B). Furthermore, in our previous study in the selective hydrogenation of furfural (C=O and C=C) [33], the Ni–B had a higher selectivity for the C=C bond in the furan ring than the Ni–P, the result did not conflict with the results of Okamoto et al. [13] which were obtained in the hydrogenation of cyclohexene and cyclo-octene (specific activity for C=C in the ring: NiB > NiP). However, the ultrafine Ni–P_x–B_y amorphous alloy catalysts, combining the effect of metalloid elements and the features of utrafine amorphous structure, demonstrate a markedly higher specific hydrogenation activity in the liquid phase hydrogenation of nitrobenzene than Raney nickel. Depending on the different function groups of the reaction compounds, by regulating the suitable P/B ratios, the ultrafine Ni–P_x–B_y amorphous alloy catalysts can be a very effective catalyst for the various liquid phase hydrogenation reactions than Raney nickel.

3.5. Catalytic surface degradation

Fig. 7 shows that when the catalyst was exposed to air, the catalyst became less active due to the formation of oxide layer on the surface [32]. The conversion–time curves of the oxidized catalysts, in which the curves in the initial time slowly rise for a period and then rapidly rise. This occurrence is attributed to that gaseous oxygen degrades the hydrogenation active sites on the oxidized catalyst surface, resulting in low initial reaction activity. However, the presence of hydrogen throughout the reaction

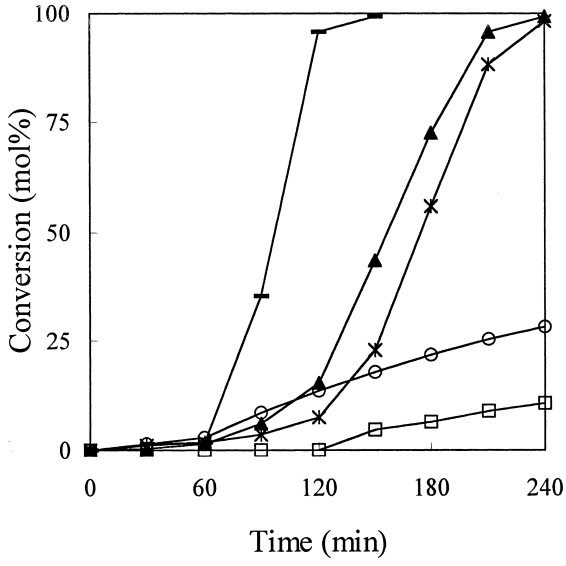

Fig. 7. Conversion-time curves for the disappearance of nitrobenzene, catalyzed by the oxidized catalyst samples. –(E) $Ni_{74.5}P_{12.1}B_{13.4}$. ▲(C) $Ni_{72.5}P_{2.0}B_{25.5}$. ∗(A) $Ni_{71.4}B_{28.9}$. ○(B) $Ni_{85.0}P_{15.0}$. □(D) $Ni_{78.5}P_{6.0}B_{15.5}$.

regenerates the degraded sites. Therefore, the reaction activity rapidly increased from initial low activity when the most degraded sites were reactivated. Furthermore, the degraded extent of the oxidized sites catalyst increasing with increasing the time of the catalyst was exposed to air, the seriously degraded sites were not easy to be reactivated.

4. Conclusion

A series of ultrafine Ni–B, Ni–P and Ni–P–B amorphous alloy catalysts with various Ni/P/B ratios was prepared by chemically reacting nickel acetate, sodium hypophosphite, and sodium borohydride in aqueous solution. Based on the results presented herein, we could conclude the following.

(1) The initial Ni/P/B molar ratio of starting materials affected the concentration of boron and phosphorus bounded to the nickel metal, resulting in the change of surface area, amorphous structure and hydrogenation activities of the catalysts.

(2) The hydrogenation of nitrobenzene to aniline catalyzed by the ultrafine Ni–P–B, Ni–B and Ni–P amorphous catalysts follows zero order with respect to nitrobenzene and first order with respect to hydrogen, which is the same as that of Raney nickel catalyst.

(3) The specific catalytic activity per surface area of the hydrogenation of nitrobenzene to aniline is in the order: sample (B) $Ni_{85.0}P_{15.0}$ > sample (E) $Ni_{74.5}P_{12.1}B_{13.4}$ > sample (C) $Ni_{72.5}P_{2.0}B_{25.5}$ > sample (A) $Ni_{71.4}B_{28.9}$ > sample (D) $Ni_{78.5}P_{6.0}B_{15.5}$ > sample (F) $Ni_{72.3}Al_{27.7}$ (Raney nickel). The modification of boron and phosphorus on the hydrogenation activity of these Ni–B, Ni–P and Ni–P–B catalysts can be ascribed to the modification of electron density on the nickel metal. In addition, the change in electron density on the nickel metal induced by boron and phosphorus modifies the activity of nickel catalyst for hydrogenation reaction. Depending on the different function groups of the reaction compounds, by regulating the suitable P/B ratios, the ultrafine Ni–P_x–B_y amorphous alloy catalysts can be a very effective catalyst for the various liquid phase hydrogenation reactions than Raney nickel.

All the prepared catalysts are easily degraded by gaseous oxygen. However, the presence of P and B passivate the surface, therefore, the catalysts did not ignite in the air.

Acknowledgements

The authors would like to thank the National Science Council of the Republic of China for financially supporting this research under contract number NSC 88-2214-E-008-008.

References

[1] J.V. Wonterghem, S. Morup, J.W. Christion, S. Charles, W.S. Wells, Nature 322 (1986) 622.
[2] A. Corrias, G. Ennas, G. Licheri, G. Marongiu, A. Musinu, G. Paschina, G. Piccaluga, G. Pinna, M.J. Magini, Mater. Sci. Lett. 7 (1988) 407.
[3] S. Linderoth, S. Morup, A. Meagher, J. Larsen, M.D. Bentzon, B.S. Clausen, C.J.W. Koch, S. Wells, S.W. Charles, J. Magn. Magn. Mater. 81 (1989) 138.
[4] S. Linderoth, S. Morup, J. Appl. Phys. 67 (1990) 4472.
[5] D.S. Xue, F.S. Li, R.J. Zhou, J. Mater. Sci. Lett. 9 (1990) 506.
[6] J. Jiang, U. Dezsi, X. Lin, J. Non-Cryst. Solids 124 (1990) 139.
[7] J. Shen, Y.Z. Hu, L.F. Zhang, Y.Z. Li, Y. Chen, Appl. Phys. Lett. 59 (1991) 3545.
[8] J.Y. Shen, Z. Hu, Y.F. Hsia, Y. Chen, Appl. Phys. Lett. 59 (1991) 2510.
[9] J. Saida, A. Inoue, T. Masumoto, Mater. Sci. Eng., A 133 (1991) 771.
[10] J.F. Deng, H.Y. Chen, J. Mater. Sci. Lett. 12 (1993) 1508.
[11] Z. Hu, J.Y. Shen, Y.N. Fan, Y.F. Hsia, Y. Chen, J. Mater. Sci. Lett. 12 (1993) 1020.
[12] H. Yamashita, H. Yoshikawa, T. Funabiki, S. Yoshida, J. Chem. Soc., Faraday Trans. I. 82 (1986) 1771.
[13] Y. Okamoto, Y. Nitta, T. Imanaka, S. Teranishi, J. Chem. Soc., Faraday Trans. I. 75 (1979) 2027.
[14] J. Deng, J. Yang, S. Sheng, H. Chen, G. Xiong, J. Catal. 150 (1994) 434.
[15] J.Y. Shen, Z. Hu, Q. Zhang, L.F. Zhang, Y. Chen, J. Appl. Phys. 71 (1992) 5217.
[16] H.C. Yao, P.H. Emmett, J. Am. Chem. Soc. 84 (1962) 1086.
[17] M.A. Aramendia, V. Borau, J. Gomez, G. Jimenez, J.M. Marinas, Appl. Catal. 10 (1984) 347.
[18] J. Wisniak, M. Klein, Ind. Eng. Chem. Prod. Res. Dev. 23 (1984) 44.
[19] H.D. Burge, D.J. Collin, B.H. Davis, Ind. Eng. Chem. Prod. Res. Dev. 19 (1980) 389.
[20] A. Metcalfe, M.W. Rowden, J. Catal. 22 (1971) 30.
[21] G.W. Pei, W.L. Zhong, S.B. Yue, X-ray Diffraction of Single, Crystalline and Amorphous Materials, Shandong Univ. Press, Jinan, 1989, p. 453.
[22] P.A. Ramachandran, R.V. Chaudhari, Three-Phase Catalytic Reactors, Gorden and Breach Science Publishers, New York, 1983, p. 15.
[23] J.J. Carberry, Physico-chemical aspects of mass and heat transfer in heterogeneous catalysis, in: J.R. Anderson, M. Boudart (Eds.), Catalysis, Science and Technology, Vol. 8, Springer, Berlin, 1987, p. 131.
[24] A. Wheeler, Reaction Rates and Selectivity in Catalyst Pores, Advances in Catalysis, Vol. 3, Academic Press, New York, 1951, p. 249.
[25] P.B. Weisz, D.C. Prater, Interpretation of Measurements in Experimental Catalysis. Advances in Catalysis, Vol. 6, Academic Press, New York, 1954, p. 143.
[26] H. S. Folger, Elements of Chemical Reaction Engineering, Prentice-Hall, Englewood Cliffs, NJ, 1992, p. 670.
[27] G.W. Roberts, The influence of mass and heat transfer on the performance of heterogeneous catalysis in gas/liquid/solid systems, in: P.N. Rylander, H. Greenfield (Eds.), Catalysis in Organic Synthesis, Academic Press, New York, 1976.

[28] Y. Okamoto, Y. Nitta, T. Imanaka, S. Teranishi, J. Chem. Soc. Faraday Trans. I 76 (1980) 998.
[29] Y. Okamoto, Y. Nitta, T. Imanaka, S. Teranishi, J. Catal. 64 (1980) 397.
[30] M. Pelavin, D.N. Hendrickson, J.M. Hollander, W.L. Jolly, J. Phys. Chem. 74 (1970) 1116.
[31] C. Li, Y.W. Chen, W.J. Wang, Appl. Catal. 119 (1994) 185.
[32] J.A. Screifels, P.C. Maybury, W.E. Swartz Jr., J. Catal. 65 (1980) 195.
[33] S.P. Lee, Y.W. Chen, Ind. Eng. Chem. Res. 38 (1999) 2548.